Random-field Potts Model for the Polar Domains of Lead Magnesium Niobate and Lead Scandium Tantalate

by

H. Qian and L.A. Bursill

School of Physics, The University of Melbourne, Parkville, Vic., 3052
Australia

Received

Abstract

A randon field Potts model is used to establish the spatial relationship between the nanoscale distribution of charged chemical defects and nanoscale polar domains for the perovskite-based relaxor materials lead magnesium niobate (PMN) and lead scandium tantalate (PST). The random fields are not set stochastically but are determined initially by the distribution of B-site cations (Mg,Nb) or (Sc,Ta) generated by Monte Carlo NNNI-model simulations for the chemical defects. An appropriate random field Potts model is derived and algorithms developed for a 2D lattice. It is shown that the local fields are strongly correlated with the chemical domain walls and that polar nanodomains tend to nucleate about the latter. The evolution of the polar domains as a function of decreasing temperature is simulated for the two cases of PMN and PST. The dynamics of the polar clusters is also discussed. The results are used in an accompanying paper (Qian and Bursill, Inter. J. Mod. Phys. B, xx, xxxx-xxxx 1996) in order to predict the temperature and frequency dependence of the dielectric response of these two relaxors.

1. Introduction

In refs.[1-4] we studied the chemical domain textures of lead scandium tantalate (PST) and lead magnesium niobate (PMN) using the combination of high-resolution transmission electron microscopy (HRTEM) and Monte Carlo methods and an extended Next Nearest Neighbour Ising model analysis. Atomic structural models for B-site cation distributions of the ABO_3 perovskite related structures were proposed and confirmed by comparison with the experimental HRTEM images. Based on these atomic models we now seek to establish the relationship between the nanoscale distribution of charged chemical defects and the nanoscale polar domain textures and their spatial and temporal fluctuations as a function of temperature. In this paper the influence of the chemical defects on the formation and dynamics of polar domains is studied. Firstly, some statistical theories of structural phase transition are critically reviewed and some non-periodic factors or randomness are introduced into the theory to allow the relaxor system to be discussed. Secondly, a random field Potts model for perovskite relaxor systems is proposed. The random fields are not set stochastically but are determined by the distribution of the B-site cations. An approximate method to calculate the random fields is proposed. Thirdly, the algorithms and procedures to conduct Monte Carlo simulations on this model and the results of simulations on a 2D lattice are presented. Finally discussions of the dynamics of the clusters and directions for further work on a three-dimensional Potts model complete this paper. In the accompanying paper[5] the dielectric permittivity and dissipation factor of the typical relaxors PMN and PST are predicted as a function of both temperature and frequency, which results are in good agreement with the experimental measurements.

2. Some statistical theories of structural phase transitions

We first give a brief description of some statistical theories of structural phase transitions as originally developed for simple, translationally invariant ferroelectrics, i.e. these have almost perfect structural order. To investigate disordered systems, some randomness is introduced into the formalism to allow the relaxor systems to be discussed. Short introductions to spin glass theory, random field theory and percolation theory are also given in this section.

(a) Model Hamiltonian

The starting point of a statistical theory is a simple model Hamiltonian. Its value is well established in solid state physics. The basic model Hamiltonian which describes structural phase transitions takes advantage of the fact that such transitions are often associated with the rearrangement of only a few atoms in the unit cell, whereas the positions of the other atoms are relatively undisturbed. Thus for a simple model it seems essential to take account only of these particular coordinates while treating the rest of the crystal lattice as a heat bath. In this manner, a model Hamiltonian can be written[6]

$$\mathcal{H} = \sum_l \{\frac{1}{2}\pi_l^2 + V_l(\xi_l)\} - \frac{1}{2}\sum_l \sum_{l'} v_{ll'}\xi_l\xi_{l'} \qquad (1)$$

where π_l and ξ_l are the generalised momentum and displacement respectively of unit cell l; $V_l(\xi)$ is the local potential function, it can be anything from quasi-harmonic to deep double-well form. We write $V_l(\xi_l)$ rather than $V(\xi_l)$ here to allow some random systems such as relaxor solutions to be approached. Besides the randomness imposed on the local potential function $V_l(\xi_l)$, the interaction parameter $v_{ll'}$ may also have a random distribution.

This model Hamiltonian is of great value for its generality and simplicity. There are plenty of applications on ferroelectrics that start with the Hamiltonian Eq. (1). For example, it has been applied to study the defect-density dependences of Curie temperatures[7,8]. On the other hand, by the rather drastic approximation of excluding all local modes except that one deemed to characterise the transition, use of Eq. (1) in its basic form precludes any discussion of coupling to other modes. In particular the coupling to acoustic modes and to elastic strains is absent. Nevertheless the model Hamiltonian Eq. (1) is readily embellished to allow for such coupling and the basic single-mode theory can be expanded to describe these phenomena.

The potential function in Eq. (1) is made up of both local terms $V_l(\xi_l)$ and inter-cell interaction term $v_{ll'}\xi_l\xi_{l'}$. The absence of either would render the Hamiltonian exactly soluble at least in principle. Thus for $v_{ll'}\xi_l\xi_{l'} = 0$ the problem reduces to one of non-interacting localised motion, while for $V_l(\xi_l) = 0$ or $V_l(\xi_l)$ of harmonic form and translational invariance the Hamiltonian can be diagonalized in terms of running waves (phonons).

The competition between local-mode and running-wave motion is a not uncommon feature of many-body dynamics, and there are two obvious methods of attacking the problem. One is to use the running waves, or non-interacting phonons, as zeroth-order basis states and to represent local anharmonicity in terms of phonon-phonon interactions which can be statistically

approximated in some way to allow diagonalization in terms of 'renormalised' phonons. The other is to approximate statistically the interaction potential $v_{ll'}\xi_l\xi_{l'}$ in some manner which reduces the many-body Hamiltonian Eq. (1) to non-interaction cell form. Looked at from the former standpoint structural transitions are caused by lattice anharmonicities; from the latter viewpoint they are precipitated by inter-cell forces. Both pictures are informative. But in relaxor systems, none of the above approximations are quite valid. The events in relaxors seem to happen in a mesoscopic scale. They cannot be described by either local model or phonon.

(b) Mean-field theory and the soft-mode concept

Within the mean-field approximation, the Hamiltonian Eq. (1) is reduced to a non-interacting form. We consider a representative cell l and, in particular, those local-model co-ordinates π_l, ξ_l which describe the phase transition of interest, replacing all other cells by their thermally averaged states. Thus in Eq. (1) we replace operators $\xi_{l'}$, for all $l' \neq l$, by their thermal averages $\langle\xi_{l'}\rangle$ which are to be determined self-consistently.

For a disordered system, we can take another approximation by decomposing the local potential function into two parts, one with translational invariance, the other without,

$$V_l(\xi_l) = V(\xi_l) - h_l\xi_l \tag{2}$$

where $V(\xi_l)$ is the contribution of the periodic part of crystal, and $-h_l\xi_l$ is the contribution of randomly distributed impurities, chemical disorder, etc. Here only the linear term of ξ_l is included and the high order terms are neglected. We can recognise that the linear term is the contribution of random fields h_l.

Now we can define a mean-field Hamiltonian for the lth cell in the form

$$\mathcal{H}_l(\mathrm{mf}) = \frac{1}{2}\pi_l^2 + V(\xi_l) - h_l^{eff}\xi_l \tag{3}$$

where

$$h_l^{\mathrm{eff}} = h + h_l + \sum_{l'} v_{ll'}\xi_l\langle\xi_{l'}\rangle.$$

We have included a term describing the introduction of a uniform static field h. This field in general is an internal field and may differ from a corresponding externally applied field if long-range (e.g. dipolar) forces are included in $v_{ll'}$. (However, if we assume needle-shaped macroscopic specimens with field parallel to the long axis, the difference vanishes and we can refer to h as an applied field without ambiguity.) The interactions have been replaced by an

effective field of magnitude $\sum_{l'} v_{ll'}\langle\xi_{l'}\rangle$. In this way the many-body problem has been reduced to one of an ensemble of independent single-ion oscillators.

If $h_l^{\rm eff}$ is distributed randomly over different unit cells, unit cell l will not be a good representative of all the other cells. Then we have two distinct kinds of averages to perform: the usual 'thermal average' and the average over the distribution of random parameters. How to calculate the average is one of the key statistical problems in spin glass theories.

On the other hand, if $h_l^{\rm eff}$ is independent of unit cell, i.e., the system has translational invariance, we can use familiar statistical results for the thermal averages. For example, some numerical results have been given by Lines[9] for a local potential with simple quartic stabilising anharmonicity

$$V(\xi_l) = \tfrac{1}{2}\omega_0^2\xi_l^2 + A\xi_l^4 \tag{4}$$

where ω_0^2 and A are both positive constants. A transition to an ordered phase is found at finite temperature if $v(0) > \omega_0^2$ ($v(0) = \sum_{l'} v_{ll'}$). It is always of second order for potentials given by Eq. (4) and a Curie temperature can be given in terms of parameters A, ω_0^2 and $v(0)$. The static uniform susceptibility $\chi(0)$ is found to be of limiting Curie-Weiss form as $T \to T_c$ with

$$\chi(0)^{-1} = \beta(T - T_c),\ T > T_c$$

and

$$\chi(0)^{-1} = 2\beta(T_c - T),\ T < T_c$$

The factor of 2 difference between the constants of the paraelectric phase and the ferroelectric phase is familiar from the thermodynamic theory of ferroelectricity.

The physical picture is one of competition between a local constraint (ω_0^2) favouring a high-symmetry phase with $\langle\xi\rangle_0 = 0$ and an interaction field ($v(0)$) preferring an ordered phase. For values $\omega_0^2/v(0) > 1$ the interaction is too weak to overcome the local constraint at any temperature and the high-symmetry phase remains stable right down to absolute zero. When $\omega_0^2/v(0) < 1$ the ordered phase is stable at low temperatures but is destroyed by the thermally induced disorder as the temperature is raised.

Phase-transition dynamics can also be discussed within mean field theory by studying the response of the mean-field equilibrium state to a time-dependent external influence. The procedure is similar to the static case. First, the behaviour of the single-cell displacement coordinate ξ_l is considered in the absence of intercell forces. A single cell response of a damped-harmonic-oscillator has the form

$$\chi_s(\omega) = \chi_s(0)\frac{\Omega_s^2}{\Omega_s^2 + i\Gamma\omega - \omega^2} \tag{5}$$

where Ω_s is a resonance frequency in the absence of damping and Γ is a damping constant. Such a form is often an excellent approximation for single-well local potentials. Then, the intercell interactions are introduced in a mean-field manner and the collective susceptibility is introduced through Fourier transforms. It can be shown that the static susceptibility will diverge at a temperature, and this divergence is associated with a soft mode.

Note that the above arguments are only valid for systems with translational invariance. For relaxor systems the translational symmetry does not exist so the above discussion cannot be applied. If we still use the language of soft modes, the promising picture of the general dynamics is perhaps one of a marginally softening lattice mode which, on softening, interacts increasingly with the defects. This interaction would produce a frequency-dependent relaxation which has the effect of slowing and eventually stopping the lattice mode softening. However, the discussion in this framework no longer has any advantage and some other framework has to be used.

(c) Deep double well limit and the Ising model

If the potential $V(\xi_l)$ (Eq. 2) has a form of deep double wells with negligible tunnelling field only two degenerate eigenstates per cell enter the statistical problem; the generalized coordinate ξ_l can be described by a dipole moment σ_l flipping between the two equivalent orientations. In this limit the mean time of two successive flippings is orders of magnitude larger than the time scale of atomic vibrations in the solid, so the phonons can be reasonably well approximated as a heat bath, as far as the flippings are concerned. Hence, the first sum of Eq. (1) will not appear explicitly in the model Hamiltonian. The potential $V(\xi_l)$ acts as a constraint and the kinetic energy is absorbed into the thermal bath. All the dynamic effects of the resulting model Hamiltonian are then due to the interactions with the surrounding thermal bath which produce thermal hopping and ensure equilibrium in the steady state. Now, we only need be concerned about the second sum in Eq. (1), i.e., the interactions between the lattice cells. Thus, we approach an Ising situation with model Hamiltonian

$$H = -2\sum_{l}\sum_{l'} v_{ll'}\sigma_l\sigma'_l - \sum_{l}\sigma_l(h + h_l) \tag{6}$$

where h_l is the local field (see Eq. 2), h is the applied field, and σ_l can be considered to be the dipole moment of the lth cell.

Generally, the interaction parameter $v_{ll'}$ is of unknown range and is directionally dependent. Even if we assume that the bilinear formalism is applicable (in general this potential can be quite complicated and perhaps not

even expressible as a sum of pairwise interactions), the complications of the $v_{ll'}$ make structural transition theory more difficult than that of conventional magnetic models.

For the case where $h_l = 0$ and $v_{ll'}$ is of translational invariance and takes a simple nearest-neighbour-only form, one- and two-dimensional models are exactly soluble, the latter being one of the rare many-body problems which is both exactly soluble and exhibits a phase transition. Even in three dimensions the use of high- and low- temperature series expansion techniques has enabled the thermodynamic singularities near T_c to be quantitatively explored with great precision.

When translational invariance is destroyed as a result of compositional fluctuations in solid solutions, the interactions $v_{ll'}$ between cells as well as the local field h_l may have a random distribution. Therefore, the behaviours of these systems become extremely complicated.

(d) Spin glass, orientational glass and random field

If the h_l at any site are comparable to or larger than $v_{ll'}$, then disorder will prevail at any temperature, since every dipolar moment tends to align with the local random field. When the h_l are much smaller than $v_{ll'}$, we have two typical models as follows

- **orientational glass model** : $h_l \ll v_{ll'}$ and $v_{ll'}$ distributed randomly; both ferro- and antiferro-type interactions are possible.
- **random field model** : $h_l \ll v_{ll'}$ and the interaction $v_{ll'}$ is predominately of ferro- or antiferro-type.

Although orientational glasses are not simply analogous to spin glasses, most of the theoretical results of spin glass theory can be applied to orientational glasses. Reference may be made to Hochli et al[11] for experimental evidence and to the review of Binder and Reger[12] for the theory of orientational glasses. We can get a basic picture of polar glasses by examining the spin glass concept here (see e.g. monograph of Fischer and Hertz[13]). The simplest definition of spin glass is that it is a collection of spins whose low-temperature state is frozen and disordered, rather than the uniform or periodic patterns we are accustomed to finding in conventional magnets. The frozen disorder means a state where the local spontaneous magnetisation $m_l = \langle S_l \rangle$ at a given site l is nonzero, though the average magnetisation $M = N^{-1} \sum_l m_l$, as well as any 'staggered' magnetisation $M_K = N^{-1} \sum_l e^{-iK \cdot r_l} m_l$, vanishes. It appears that, in order to produce such a state, two ingredients are necessary : there

must be competition among the different interactions between moments, in the sense that no single configuration of the spins is uniquely favoured by all the interactions (this is commonly called 'frustration'), and these interactions must be at least partially random. These facts suggest that the spin glass state is intrinsically different from conventional forms of order and requires new formal concepts to describe it. Some useful concepts among others are broken ergodicity, new definition of order parameters, many-time-scale dynamics, etc.

Note that the polar glass model proposed by Viehland et al.[13] for PMN may have a different content to the above glass model. The basic elements of that model were the polar clusters rather than the unit cells. From the point of view of statistical mechanics, their model was established on the rescaled lattice of PMN by the linear size of the polar clusters. The source of the randomness of the interactions among the polar clusters was not clarified in the model.

The randomness of the interactions between cells in a random field model is less than in a polar glass model, so the second case is closer to an ordinary structural phase transition. According to the work of Imry and Ma[14], random fields may play a role to destroy the second-order phase transition and stabilise the domain states on mesoscopic length scales. The basic idea is that the energy gain of a reversed domain favoured by the direction of a mesoscopic fluctuation of the random fields will compensate the energy loss due to the interface between the reversed domain and its bulk surrounding. This was the model that Kleemann[15] applied to PMN.

(e) Introduction to percolation theory

Few theoretical techniques are available for dealing with severely disordered systems; percolation theory is one of the nicest of these techniques (see e.g. Zallen[16] or Stauffer[17]). It provides a well-defined, transparent and intuitively satisfying model for spatially random processes, and can be applied to a broad range of physical phenomena. Most interestingly percolation models present sharp phase transitions at which long-range connectivity suddenly appears.

Percolation theory deals with the interconnections of elements in a system. There are two basic types of percolation processes: bond percolation and site percolation. A ferromagnetic crystal which is diluted by random substitution of non-magnetic for magnetic ions is a good example of site percolation. Let us look at the character of the system at $0K$, when the dilution $1-p$ is varied (p is the fraction of magnetic ions). At $T = 0K$, the pairwise

coupling between two neighbouring magnetic atoms is certain, i.e., their spins must be parallel, so that the undiluted pure system is a ferromagnet with all spins parallel and all magnetic ions in the same cluster and contributing to the macroscopic magnetization M. In other words, two neighboured spins are always connected by a bond and surely belong to the same cluster. When p decreases, with the addition of nonmagnetic ions, M also decreases. When p falls below p_c, the site-percolation threshold for the lattice, M vanishes. All of the magnetic ions now occur in finite clusters. Although within each cluster all spins are coupled, the separate clusters can independently reorient so that the net magnetization cancels out on a macroscopic scale.

Thermal phase transitions in an Ising system can be viewed as bond percolation. At zero temperature, the parallel alignment of adjacent spins is mandated by the nearest-neighbour exchange coupling. When we "turn on" the temperature to a finite value, the nonvanishing Boltzmann factor $\exp(-J/kT)$ permits the occurrence of low energy configurations in which a few spins are flipped. The complement of the Boltzmann factor $1 - \exp(-J/kT)$, which is a function of temperature T, plays the part of the bond-probability p. Eventually, at very high temperature ($kT \ll J$), adjacent spins decouple completely as the Boltzmann factor approaches unity and the exchange-induced bias in favour of parallel spins disappears. In between, at critical temperature T_c, which is of order J/k, the solid ceases to be a ferromagnet.

While the connection between site percolation and variable-composition magnet alloys is really quite close, the analogy between bond-percolation and the thermodynamic ferromagnetic/paramagnetic (F/P) transition is looser. There are very strong correlations between spins in the F/P transition. A non-correlated bond-percolation process can not exactly describe the behaviour of correlated spins. For example, while the interaction (or "bond-probability") between two adjacent parallel spins is $p = 1 - \exp(-J/kT)$, it should be zero for two anti-parallel spins. Thus the percolation problem in an Ising model should be both bond- and site-related. Some more complicated correlated percolation models are needed for this purpose. The Fortuin-Kasteleyn transformation[18] maps a Potts model into a bond-site correlated percolation problem. It has been used to construct cluster algorithms for Monte Carlo simulation of the Potts model and the Ising model. This will be discussed in detail below.

3. A random field Potts model for relaxors

It has been shown that the local polarization ($P_s \neq 0$) in PMN exists for temperatures far above the permittivity maximum T_m[19,20]. There are certainly more than two orientations for local polarization in any known relaxor, so the Ising model is not a suitable description for these systems. The most likely orientations of local polarization for PMN and PST can be 8 ⟨111⟩ directions, 12 ⟨110⟩ directions and 6 ⟨100⟩ directions of the cubic Pm3m cell. For concreteness in the discussion, we simply assume here that the local polarization takes the 8 ⟨111⟩ directions. Considering the experimental[21,22] and theoretical[23] evidence, this may be the actual case for PMN and PST. However the results drawn in this section will not depend significantly on this assumption.

In the light of the deep double-well limit (Sec.2(c)), we assume the potential $V(\xi_l)$ has an eight-well form with each well located in one of the ⟨111⟩ directions of the Pm3m cell. As indicated in Sec.2(c), the parameter $v_{ll'}$ which describes the interaction between two unit cells may have a very complicated form. As for PMN and PST nanoscale polar domains have been observed in a large temperature range, so the interactions should be predominantly ferroelectric, at least in short range. For simplicity we only take into account the interactions between nearest neighbours and assume $v_{ll'}$ takes the form of Potts model[24]:

$$v_{ll'}\sigma_l\sigma_{l'} = -J\delta(\sigma_l, \sigma_{l'}) \tag{7}$$

where

$$\begin{aligned} \delta(\sigma_l, \sigma_{l'}) &= 1 \quad \text{if} \quad \sigma_l = \sigma_{l'} \\ &= 0 \quad \text{if} \quad \sigma_l \neq \sigma_{l'} \end{aligned} \tag{8}$$

Thus, we have

$$\mathcal{H} = -J\sum_{ll'}\delta(\sigma, \sigma') + \sum_l h_l\sigma_l \tag{9}$$

This is actually a random field Potts model.

When the state of Potts model is equal to 2, Potts model is equivalent to the zero-field Ising model which has been solved exactly by Onsager[25]. There are some other special cases where Potts model can be exactly solved. But for systems with dimension higher than 2, there is no exact solution. However, Monte Carlo simulations can give some interesting results for this model.

Srolovitz and Scott[26] have initially applied four-state (scalar) Potts models and four-state clock model (vector Potts models) on ferroelectrics. Their

models are two-dimensional. They analysed the vertex topography for antiphase boundaries (APBs) and showed that in barium sodium niobate the vertices are all fourfold and thus are describable not by a four-state scalar Potts model but by a clock model.

It is worthwhile to indicate that we do not intend to deal with the genuine ferroelectric phase transition here. We ignore the ferroelectric and ferroelastic distortions in our models. Hence our model will not give any displacive characteristics of the systems. For PMN and PST-def[2] that is not a problem, because the low temperature phases remain cubic macroscopically.

Usually, random fields h_i are set randomly site by site, i.e., there is no correlation even between nearest neighbours. This is not a realistic representation of the relaxor systems. Instead the random fields should be determined by the distribution of B-site cations in perovskite relaxors. In refs.[3,4] we have analysed the frozen structural states of PMN and PST. Here we propose a simple model to set up the random fields at A-sites, starting from the distribution of the B-site cations.

Fig 1 shows an A-site cation (Pb^{2+}) surrounded by eight B-site cations (Mg^{2+} and Nb^{5+}). It experiences a local electric field due to the non-symmetrical distribution of Mg^{2+} and Nb^{5+} ions on the eight corners of the cubic unit cell. The electric field acting on Pb^{2+} can be determined by vector summation of the components in four pairs of cubic diagonal directions. If the pair of cations at the cubic diagonal positions are the same, the electric field in this direction will be zero. For simplicity the contribution of the cations beyond next nearest neighbours is not considered here, which should not influence significantly the overall characteristics of the distribution of random fields. This model can be formalized as below for computer simulations.

The configuration of the B-site cations can be described by a matrix $B(i,j,k)$ where i, j and k are the position index of lattice cells. $B(i,j,k)$ takes a value either 1, for Nb^{5+} , or -2, for Mg^{2+}. Eight B-sites $B(i,j,k)$, $B(i+1,j,k)$, $(B(i,j+1,k)$, $\cdots$, $B(i+1,j+1,k+1)$ form a cubic cell. The local electric field at the centre of the cubic cell (i.e. A-site) can be determined by four components in $\langle 111 \rangle$ directions:

$$\begin{cases} E1 = B(i+1,j+1,k+1) - B(i,j,k) \\ E2 = B(i,j+1,k+1) - B(i+1,j,k) \\ E3 = B(i+1,j,k+1) - B(i,j+1,k) \\ E4 = B(i,j,k+1) - B(i,j,k+1) \end{cases} \tag{10}$$

$E1$, $E2$, $E3$ and $E4$ can have different values, 3 for Nb–Mg pairs, 0 for Nb–Nb or Mg–Mg pairs and -3 for Mg–Nb pairs. Here we are only concerned

with the relative strength. Assuming the local electric field at the A-site is $E(i,j,k)$, we have its three components

$$\begin{cases} E_x(i,j,k) = E1 - E2 + E3 - E4 \\ E_y(i,j,k) = E1 + E2 - E3 - E4 \\ E_z(i,j,k) = E1 + E2 + E3 + E4 \end{cases} \tag{11}$$

Again, they are relative strength. Eqs. (10) and (11) are not limited to PMN. They can be applied to any complex perovskite-type structures, e.g. PST.

It is easy to understand that the local field on the boundary of B1-rich or B2-rich clusters should be very strong, whereas it should be relatively weak inside the clusters. In PMN due to the existence of negatively charged $(Pb_2MgNbO_6)^{1-}$ clusters (1:1 ordering with doubled unit cell) and positively charged $(PbNbO_3)^{1+}$ clusters[4] the strength of the electric field may fluctuate from place to place. Let us consider the local electric fields experienced by the lead cations. The electric fields in the centers of $(Pb_2MgNbO_6)^{1-}$ clusters or $(PbNbO_3)^{1+}$ clusters will be very weak because the Pb^{2+} ions have local environment with cubic symmetry. On the other hand, the electric fields on the boundaries of the charged clusters may be expected to be much stronger.

Upon establishment of the relationship between the frozen distribution of the B-site cations and random fields, we can now use the random field Potts model to simulate the influence of the chemical domain texture on the formation and dynamics of the polar domains.

4. Monte Carlo Simulations

In refs.[2-4] we used a spin-exchange algorithm to simulate the ordering process of a binary solid solution. To simulate a ferromagnetic or ferroelectric phase transition, one needs to use spin-flip algorithms. Those commonly used are the Metropolis single spin-flip algorithm. However, conventional Metropolis algorithms face the difficulty of critical slowing down as the critical temperature is approached. Among many algorithms proposed to overcome the critical slowing down problem, Swendsen–Wang and Wolff cluster algorithms are widely used. In addition, one may expect that the cluster concept used in the algorithms have some relationship with the so-called superparaelectric polar clusters[27]. Hence, we will use cluster algorithms in the simulations.

(a) Algorithms and simulation procedures

(i) Swendsen–Wang Cluster algorithms

Swendsen and Wang[28] apply the Fortuin-Kasteleyn (FK) transformation[18] directly to the spin configurations, to construct a new Monte Carlo algorithm. The FK transformation consists of replacing each interaction between the spins on two sites by either a "bond" (requiring the spins on these two sites to be identical) with a probability $p = 1 - \exp(-J/kT)$, or "no-bond" with a probability $1 - p$. This transformation is performed on all interactions leaving only configurations of bonds forming clusters. All spins on a given cluster must have the same value, but the value is independent of the spins on any other cluster. This problem, with both spins and bonds present, is known as "site-bond percolation".

The probability distribution of configurations in a Potts model can be written as

$$P(\sigma) = \frac{1}{Z} \exp(K \sum_{(i,j)} (\delta_{\sigma_i,\sigma_j} - 1), \tag{12}$$

where $K(= J/k_BT)$ is the coupling strength; $\sigma_i = 1, 2, \cdots, q$; the sum runs over nearest neighbour pairs; Z is the partition function. A SW Monte Carlo move consists of two steps: the first step transforms a Potts configuration to a bond configuration; the second transforms back from bond to a new Potts configuration.

- step 1: Create a bond, $n_{ij} = 1$, between neighbours site i and j stochastically with a probability $p = 1 - e^{-K}$, if $\sigma_i = \sigma_j$. No bond will be present otherwise, the bond variable sets to $n_{ij} = 0$.

- step 2: Identify clusters as sets of sites connected by bonds, or isolated sites. Two sites are said to be in the same cluster if there is a connected path of bonds joining them. Each cluster is assigned a new Potts value chosen with equal probability among 1 to q. The Potts variable σ' now takes the value of the cluster it belongs to. By erasing the bonds, we are left with a new Potts configuration. The new configuration can differ substantially from the original one, since large clusters can be changed in a single step.

The algorithm is highly ergodic, since every state can be reached from any other state in one move with a non-zero probability. The steps 1 and 2 leave the probability distribution Eq. (10) invariant.

(ii) Wolff cluster algorithm

The SW algorithm has been modified and generalized by Wolff[29] in the form of a single-cluster method. The essential idea is to choose randomly

a site i and consider only the cluster around that site. The neighbours of the chosen center site are included as a member of the cluster with the same probability as that in SW. This process continues until no more new sites are generated, i.e., the perimeter of the cluster is reached. The Wolff single-cluster algorithm is more efficient than the SW algorithm in higher dimensions.

(iii) Algorithm for random field Potts model

To apply cluster algorithms to the random field Potts model one has to find a scheme to take into account the random fields. Dotsenko, Selke and Talapov[30] have proposed a method for a random Ising model. Independently of[30], we generalized their method for our random field Potts model. One may construct clusters the same way as in SW or Wolff algorithm and flip the cluster according a probability determined by the local random fields:

$$p_c = \frac{\exp(\mathrm{h}_c \cdot \sigma_c / kT)}{\sum_q \exp(\mathrm{h}_c \cdot \sigma_q / kT)} , \tag{13}$$

where

$$\mathrm{h}_c = \sum_{i \in C} \mathrm{h}_i , \tag{14}$$

C denotes the cluster, h_i is the random field at site i, σ_q takes all the Potts orientations and σ_c is the orientation of the cluster.

Simulations can start with the setting-up of the random fields from the B-site cations. The atomistic models obtained by use of NNNI and eNNNI models[3,4] are first used to set up the distribution of the B-site cations. Then the random fields on the A-sites are calculated according to the method we proposed above. After that we ignore the existence of the B-site cations and oxygens and are only concerned with the random fields and the dipole moments on A-sites. Finally the Potts values for each A-site are initialized and the standard Monte Carlo procedures are followed to conduct the simulations. The Potts values can be initialized either randomly to simulate the cooling processes, or with a single polar domain to simulate the heating processes after a field-cooling process.

4. Simulation results

(a) Calculation of the local electric fields

As a first step the simulations are performed on a 2D square lattice up to size 100 × 100. Fig. 2 shows the lattice occupied by A-site dipolar moments

and B-site cations B1 and B2, which is similar to the structure of PMN in 3D. The ratio of the B-site cations B1 and B2 is 1:2. The charges of B1 and B2 are set to be -2 and 1 respectively. A-sites are occupied by dipolar moments with 4 possible orientations in the diagonal directions. These dipolar moments represent the shift of Pb^{+2} relative to the O^{-2} and B-site cations in PMN.

Figs. 3 show two kinds of B-site cation distributions with 1:2 ratio of B1 and B2 and the calculated x and y components of local electric fields at the A-sites (E_{lx} and E_{ly}). The 1:2 ratio of B1 and B2 is similar to that of PMN in 3D. Fig. 3 (a) is a completely random distribution while (b) and (c) are the corresponding E_{lx} and E_{ly} distributions respectively. Fig. 3 (d) is a configuration obtained from the Monte Carlo simulation of the extended NNNI model (see ref.[4]) and (e) and (f) are the E_{lx} and E_{ly} distributions respectively. In Fig. 3 (a) and (d) B1 and B2 ions are shown by black and white squares respectively. One can easily see in (d) the 1:1 ordering clusters of B1 and B2 (chess board patterns) and the B2-clusters (white regions), which is the typical case for PMN in 3D. The average linear size of these clusters is about 15×15 unit cells. In Fig. 3 (b), (c), (e) and (f) black (solid squares) represents positive direction, white means zero and grey (crosses) means negative. These local electric fields are calculated with the method proposed in Sec. 3(b). It is shown that the local field distribution (b and c) due to a complete random B-site distribution (a) is also random, virtually site by site. However, if B-site 1:1 ordering occurs the local field distribution generated by the B-site distribution (d) is not random site by site; the local field inside a 1:1 ordering cluster or a B2-cluster is close to zero and the the local field on the boundary of these two clusters is very strong. Hence, the local fields are correlated in direction and strength, with a correlation length similar to that of the size of 1:1 ordering clusters.

Figs. 4 simulate two cases in PST where the B-site ratio is set to be 1:1. Fig. 4 (a) is a configuration with average size of 1:1 ordering cluster 15, which is chosen to simulate the typical PST-d specimen[3], (b) and (c) are respectively the local electric field distributions E_{lx} and E_{ly} corresponding to (a). The scale of the chemical domains in Fig. 4 (a) is similar to that in Fig. 3 (d), but the distributions of their local electric fields are somewhat different. In Figs. 3 (e) and (f) one can easily find regions where strong electric field in positive or negative dominate, but in Figs. 4 (b) and (e) the sites with strong positive local field are always compensated by the neighboured sites with strong negative local field. The reason for that is that the 1:1 ordering chemical domains in Fig. 3 (d) are charged whereas those in Fig. 4 (a) are neutral. This may underline the different behaviours of PMN and PST-d. Fig. 4 (d) is a configuration with significant long scale anti-phase boundaries,

(e) and (f) are the E_{lx} and E_{ly} due to B-site cation distribution (d). It is shown clearly that the local electric fields are concentrated on the anti-phase boundaries.

(b) Evolution of polar domain textures

Now we come to the simulation of the Potts model. For convenience of description, we can rewrite Eq. (9) as

$$\mathcal{H} = -J \sum_{ll'} \delta(\sigma, \sigma') + h \sum_{l} \gamma_l \sigma_l \,. \tag{15}$$

If σ_l and γ_l are taken to be dimensionless, then both J and h have units of energy, where J describes the strength of the interaction between two moments and h corresponds to the strength of the random fields.

Fig. 5 shows the polarization P as a function of the reduced temperature kT/J for a pure two-dimensional 4-state Potts model ($h = 0$). A sharp phase transition occurs at $kT/J \sim 0.9$. A single domain forms rapidly when the temperature is decreased below this point.

When $h > 0$ a random field stabilized domain state will appear. In this case the global polarization P is no longer a good parameter to describe the behaviour of the system. Theoretically the global polarization will stay zero for the domain state because all the possible variants of domains have same probability. So the average size of the polar cluster is chosen as a parameter for the nanodomain state. Fig 6 shows the average size s of the polar clusters as a function of the reduced temperature kT/J, where h/J is taken to be 0, 0.2, 0.3, 0.4, 0.5, 0.6, 0.8 and 1.0 respectively. The local electric distribution (Figs. 3 (e,f)) calculated from a B-site cation distribution (Fig. 3 (d)) is used for γ_l in Eq. (15). For the given distribution of the random fields γ_l the strength h determines the final size of the frozen domains. When $h = 0$ the average size should diverge at a certain temperature, for a system with infinite size, but it saturates at 10000 in a system with size 100×100. Hence the results for small h (say, $h < 0.5$) is strongly influenced by the finite size effect, where the final frozen domain size becomes comparable to the system size; the average size s may be subject to significant fluctuations from sample to sample. Fortunately the case we are interested in here is where the size of the frozen polar domains is comparable to that of the chemical domains. In this case, the size of the frozen domains is much smaller than 10000.

Fig. 7 is the enlarged figure for the case of $h/J = 1$ in Fig. 6. The frozen polar domain size at low temperature is about 15×15 unit cells in 2D which corresponds closely to the size of the chemical domains. Fig. 8(a-f)

are snap-shots of the polar moment configurations in the simulation process when $h/J = 1$. They show the evolution of the polar domain textures when the temperature is decreased : (a) is the initial random configuration, the dipolar moments are totally decoupled; (b) $kT/J = 1.0$, the average size $s = 8$; (c) $kT/J = 0.8$, $s = 25$; (d) $kT/J = 0.6$, $s = 97$; (e) $kT/J = 0.3$, $s = 205$; (f) $kT/J = 0.2$, $s = 206$. The coupling of dipolar moments starts at $kT/J \sim 1.0$. It becomes significant in the temperature range $kT/J = 0.7$ - 0.9; note that the average size increases rapidly. When $kT/J < 0.4$, the system is frozen into a domain state, the domain textures virtually remain unchanged.

(c) Relationship between chemical domains and polar domains

Fig. 9 shows a comparison between the chemical domain texture and different polar configurations of the frozen polar state at $kT/J = 0.3$ for different values of h/J (refer to Fig. 6) : (a) is the B-site cation distribution used for calculation of the local electric field on A-site (see Fig. 3 (d)-(f)); (b) $h/J = 5$; (c) $h/J = 2$; (d) $h/J = 1$; (e) $h/J = 0.8$; (f) $h/J = 0.6$. When $h \geq 2$ the polar configuration is controlled predominately by the local field; one can find the correspondences between chemical domain textures and polar domain textures (Fig. 9 (b) and (c)). Increasing h/J will not change the polar configuration. The boundaries of chemical domains act as nuclei of the polar domains. When h/J is decreased the average size of frozen polar domains at low temperature increases and the relationship between chemical domain textures and polar domain textures becomes less obvious. One can only find the correspondence in some regions(Fig. 9 (d) and (e)). This may be the case for PMN in 3D. When $h/J \leq 0.6$ the average size of the frozen polar domains becomes much larger than that of chemical domains and direct correspondence between the chemical domains and polar domains disappears (Fig. 8(f)). This may correspond to the case for PST-d in 3D.

5. Discussion

(a) Dynamics of the clusters

One may relate the cluster flipping in cluster algorithms to the "super-paraelectric polar nanodomains" in relaxor systems and give to them some microscopic explanations. The cluster used here is basically a statistical concept, it reflects the interaction of the dipole moments. Each cluster is totally independent of others due to the special way of identifying the clusters. The

cluster size is temperature and time dependent; the atoms within the cluster move together in the lifetimes of the cluster. We can refer to these clusters as dynamical. Due to the effect of the "correlated random field", some clusters may have very long lifetimes and also very compact geometry so that they can be regarded as polar nanodomains. These nanodomains have very slow dynamics because they tend to align their polarizations with the local field, so they can be classified as frozen. More complete discussions about the dynamical and frozen polar domains are given in the accompanying paper[5], where we go on to predict the frequency dependence of the dielectric response of PMN and PST.

In general, the "time" associated with the Monte Carlo steps is not related to the physical time by which a real system evolves. The Markov chain generated by the Metropolis method or SW algorithm just represents an ensemble of the system in thermodynamic equilibrium. However, in some cases, the connection between the Monte Carlo time and the physical time is certain. In the case of the NNNI model, we have connected the Markov chain generated by the Metropolis method to the actual time evolution of the diffusion of atoms in the lattice.

In the SW or Wolff algorithms the probability for a cluster to flip to the other orientations is always $1/q$ and independent of the size of the cluster. In a realistic dynamical system, there exist energy barriers between any two orientations of the clusters. These energy barriers should be proportional to the size of the clusters. A flipping cluster must gain energy from the thermal bath to overcome the energy barrier. The larger clusters need to wait for longer time to have a chance to flip. Hence, the SW and Wolff cluster algorithms are not suitable to investigate the dynamical properties of the system. To make the cluster algorithm more realistic, one can introduce a parameter θ so that the flipping probability of a cluster is $\exp(-\theta sJ/kt)$. The algorithm remains ergodic and the probability distribution remains invariant if θ takes a finite value. One can easily recognise that θJ represents the depth of wells in our deep wells model. It did not appear explicitly in the model Hamiltonian Eq. (9), because it does not influence the thermal equilibrium distribution as long as it is finite. However, it does influence the dynamical properties of a system. The introduction of θ will allow the stochastic dynamics of the algorithm to be closer to the realistic dynamical process but less efficient in studying the equilibrium characteristics. In the Metropolis algorithm, θ will be absorbed by the constant factor τ which can be chosen arbitrarily. Recently an efficient method for slow dynamical system has been proposed[31], it may also be a good algorithm for the random field Potts model.

(b) Directions for further work

The simulation results on 2D lattices have shown that the microscopic model proposed in this chapter has promising potential for the study of the relaxor system. We are at present using the results of the present simulations to calculate the bright- and dark-field HRTEM images of very thin specimens of PMN and PST, where the 2D approximation should be valid. Thus we expect to be able to develop electron optical techniques which will allow both the chemical nanodomain textures as well as the polar nanodomain textures to be extracted from the HRTEM by further development of our image processing methods (c.f. ref.[32].

In the scheme of the Potts model and Monte Carlo simulation methods presented above, a more realistic simulation for relaxor PMN and PST may be conducted for 3D. This study should lead to a good understanding of the relationship between chemical domain textures and polar domain textures. In principle, all the zero-field and non zero-field cooling and/or heating processes can be simulated. One may also be able to extract domain size distribution functions $n(s)$, directly from the simulations. (At present these are assumed to be Gaussian, without any proof, in ref.[5]. Ideally, the simulations should be conducted on a system with reasonably large size $L \times L \times L$, say $L = 200$. However, these simulations will consume extremely long CPU times even on a very high performance computer, due to the slow dynamics of the metastable domain states[33]. The simulations described above for 2D lattices were conducted on four IBM RISC 6000 workstations. One may need to use a supercomputer or find some more efficient algorithms to do the simulations for 3D.

Acknowledgements

This work was supported financially be the Australian Research Council and the Australian Equity and Merit Scholarship Scheme.

References

[1] J.L. Peng and L.A. Bursill, *Mod. Phys. Letts. B*, **7**, 609-621 (1992).
[2] H. Qian, J.L. Peng and L.A. Bursill, *Inter. J. Mod. Phys. B*, **7**, 4353-4369 (1993).
[3] L.A. Bursill, J.L. Peng, H. Qian and N. Setter, *Physica B*, **205**, 305-326 (1995).
[4] L.A. Bursill, H. Qian, J.L. Peng and X.D. Fan, *Physica B*, **216**, 1-23 (1995).
[5] H. Qian and L.A. Bursill, *Inter. J. Mod. Phys. B*, **xx**, submitted (1996).
[6] M.E. Lines and A.M. Glass, *Principles and Applications of Ferroelectrics and Related Materials*, Clarendon Press, Oxford (1979).
[7] J.F. Scott, *Phase Transitions*, **15**, 135-142 (1989).
[8] G.E. Feldkamp, J.F. Scott and W. Windisch, *Ferroelectrics*, **39**, 1163-1168 (1981).
[9] M.E. Lines, *Phys. Rev. B*, **177**, 797-811 @ 812-818 @ 819-824 (1969).
[10] U.T. Hochli, K. Knoor and A. Loidl, "Orientational Glasses" in *Advances in Physics*, **39**, 405-615 (1990).
[11] K. Binder and J.D. Reger, "Theory of Orientational Glasses: Models, Concepts and Simulations" in *Advances in Physics*, **41**, 547-627 (1992).
[12] K.H. Fischer and J.A. Hertz, *Spin Glasses*, Cambridge University Press (1991).
[13] D. Viehland, S.J. Jang, L.E. Cross and M. Wuttig, *Philos. Mag.*, **B 64**, 335-344 (1991a).
[14] Y. Imry and S.K. Ma, *Phys. Rev. Letts.*, **35**, 1399-1401, (1975).
[15] W. Kleemann, *Inter. J. Mod. Phys. B*, **13**, 2469-2507 (1993).
[16] R. Zallen, *The Physics of Amorphous Solids*, (John Wiley, New York) (1983).
[17] D. Stauffer, *Introduction to Percolation Theory*, (Taylor and Francis, London) (1987).
[18] C. M. Fortuin and P.W. Kasteleyn, *Physica*, **57**, 536-564 (1972).
[19] G. Burns and F.H. Dacol, *Phys. Rev. B*, **28**, 2527-2530 (1983).
[20] G. Burns and F.H. Dacol, *Ferroelectrics*, **104**, 25-31 (1990).
[21] N. de Mathan, E. Husson, G. Galvarin, J.R. Gavarri, A.W. Hewat and A. Morell, *J. Phys.: Cond. Matter*, **3**, 8159-8171 (1991).
[22] P. Groves, *J. Phys. C*, **18**, L1073-L1077 (1985).

[23] E. Salje and U. Bismayer, *J. Phys.: Cond. Matter*, **1**, 6967-6976 (1989).
[24] R.B. Potts, *Proc. Camb. Phil. Soc.*, **48**, 106-109 (1952).
[25] L. Onsager, *Phys. Rev.*, **65**, 117-121 (1944).
[26] D.J. Srolovitz and J.F. Scott, *Phys. Rev. B*, **34**,1815-1819 (1986).
[27] L.E. Cross, *Ferroelectrics*, **76**, 241-267 (1987).
[28] R.H. Swendson and R-S. Wang, *Phys. Rev. Letts.*, **58**, 86-88 (1987).
[29] U. Wolff, *Phys. Rev. Letts.*, **62**, 361-364 (1989).
[30] V.S. Dotsenko, W. Selke and A.L. Talapov, *Physica A*, **170**, 278-281 (1991).
[31] M.A. Novotny, *Phys. Rev. Letts.*, **74**, 1-4 (1995).
[32] X.D. Fan, H. Qian, J.L. Peng and L.A. Bursill, *Integrated Ferroelectrics*, **9**, 233-237 (1995).
[33] D. Stauffer, C. Hartzstein, K. Binder and A. Aharony, *Z. Phys. B*, **55**, 325-333 (1984).

Figure Captions

Figure 1.
Diagram illustrating a Pb^{2+} ion in the center experiences a local electrical field due to the non-symmetrical distribution of Mg^{2+} and Nb^{5+} on the eight corners of cubic unit cell.

Figure 2.
Diagram illustrating the 2D lattice used in the random field Potts model simulations, which is similar to the structure of PMN in 3D.

Figure 3.
Two kinds of B-site cation distribution with 1:2 ratio of B1 and B2 ((a) and (d)) and the calculated x ((b) and (e)) and y ((c) and (f)) components of local electric fields. See text for details.

Figure 4.
Two kinds of B-site cation distribution with 1:1 ratio of B1 and B2 ((a) and (d)) and the calculated x ((b) and (e)) and y ((c) and (f)) components of local electric fields. See text for details.

Figure 5.
The polarization P as a function of the temperature kT/J for pure Potts model. A sharp ferroelectric phase transition occurs at $kT/J \sim 0.9$.

Figure 6.
The average size s of the polar clusters as a function of the temperature kT/J, where h/J is taken to be 0, 0.2, 0.3, 0.4, 0.5, 0.6, 0.8 and 1.0 respectively.

Figure 7.
Enlarged figure for the case of $h/J = 1$ in Fig. 5. The average size of the frozen polar domains in low temperature is similar to that of the chemical domains.

Figure 8.
The snap-shots of polar moment configurations in the simulation process when $h/J = 1$, which show the evolution of the polar domain textures when the temperature is decreased.

Figure 9.
Comparison between chemical domain texture and different polar configurations in frozen polar state at $kT/J = 0.3$ for different value of h/J.

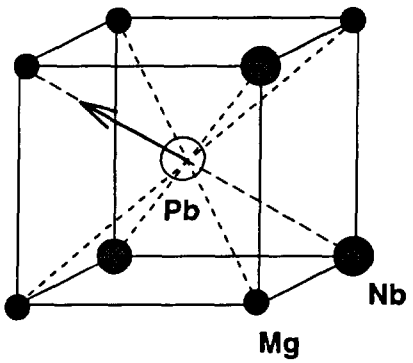

Figure 0.1: Diagram illustrating a Pb^{2+} ion in the center experiences a local electrical field due to the non-symmetrical distribution of Mg^{2+} and Nb^{5+} on the eight corners of cubic unit cell.

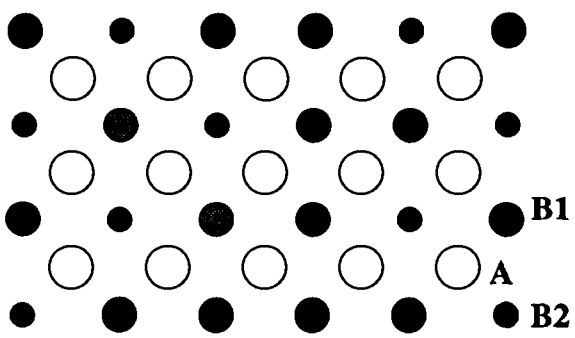

Figure 0.2: Diagram illustating the 2D lattice used in the random field Potts model simulations, which is similar to the structure of PMN in 3D.

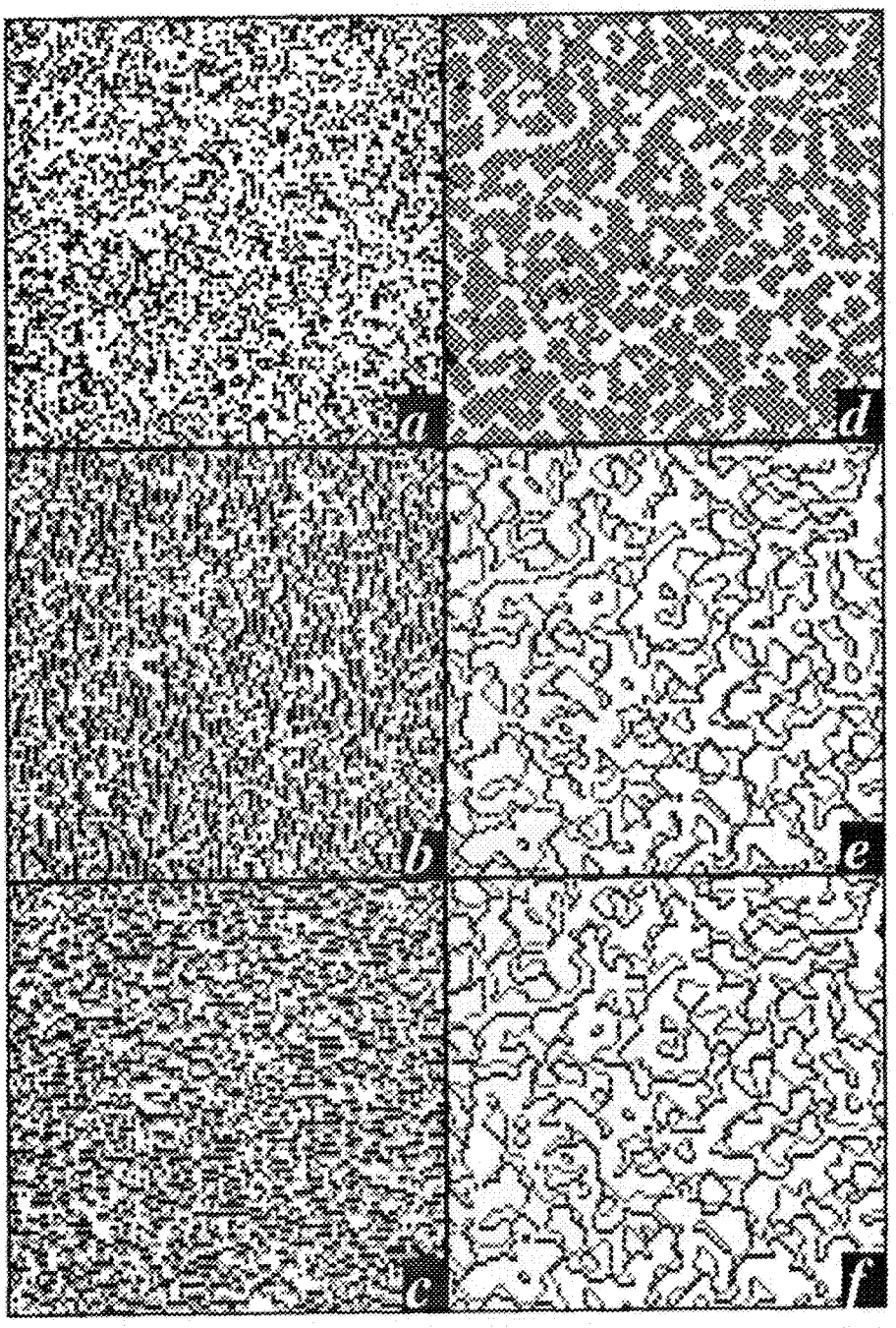

Figure 0.3: Two kinds of B-site cation distribution with 1:2 ratio of B1 and B2 ((a) and (d)) and the calculated x ((b) and (e)) and y ((c) and (f)) components of local elecric fields. See text for details.

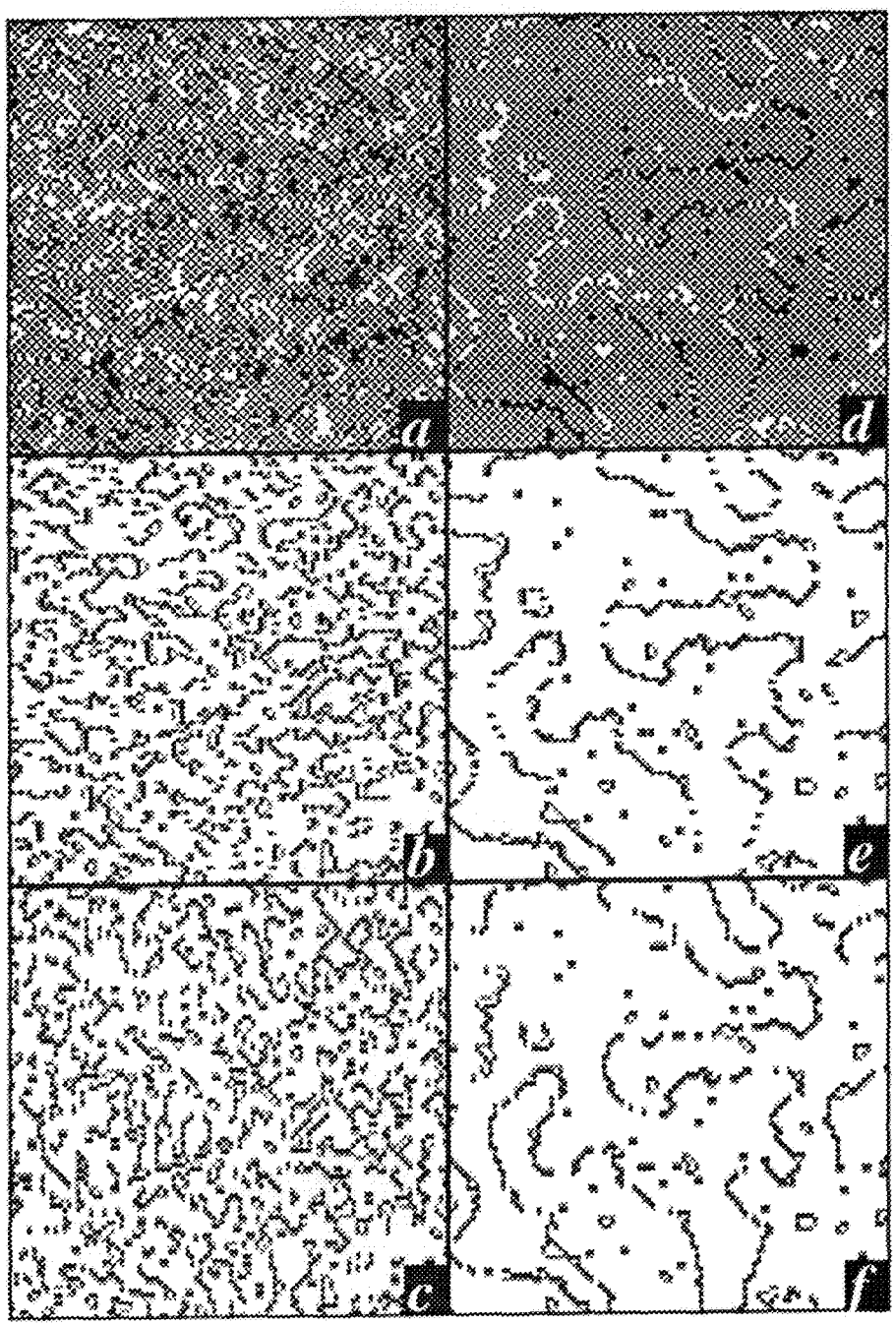

Figure 0.4: Two kinds of B-site cation distribution with 1:1 ratio of B1 and B2 ((a) and (d)) and the calculated x ((b) and (e)) and y ((c) and (f)) components of local elecric fields. See text for details.

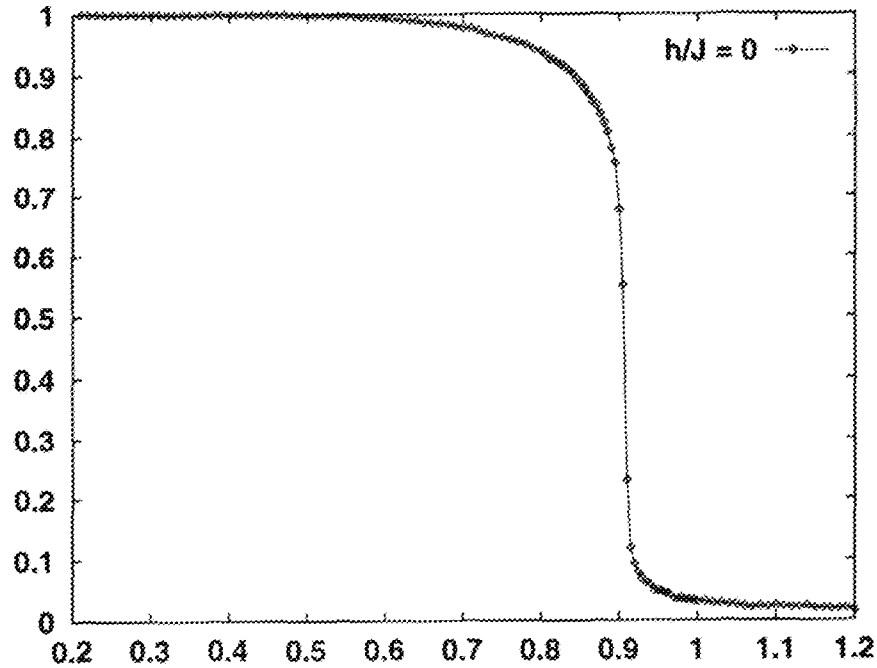

Figure 0.5: The polarization P as a function of the temperature kT/J for pure Potts model. A sharp ferroelectric phase transition occurs at $kT/J \sim 0.9$.

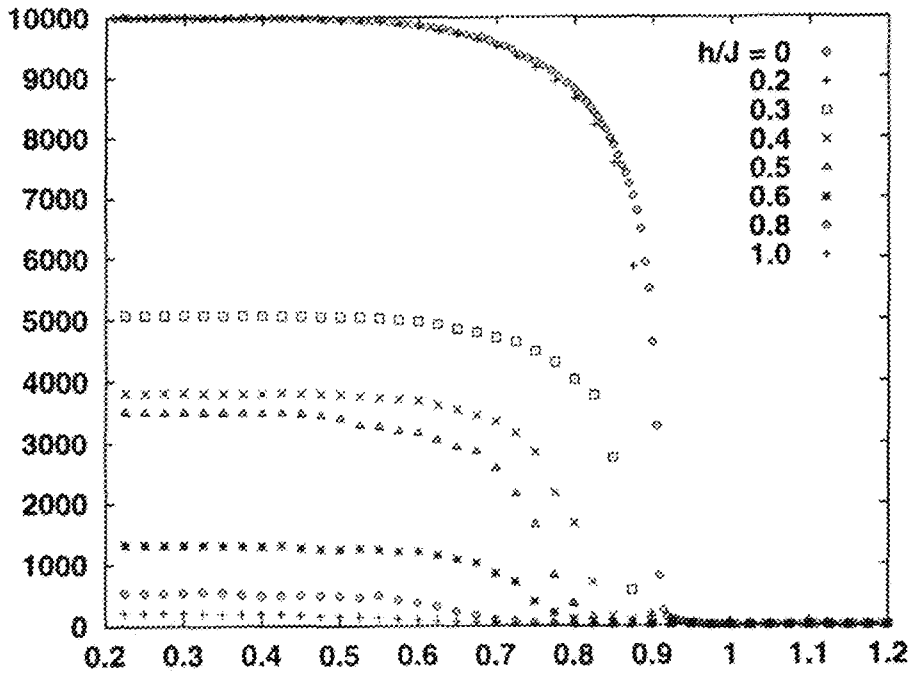

Figure 0.6: The average size s of the polar clusters as a function of the temperature kT/J, where h/J is taken to be 0, 0.2, 0.3, 0.4, 0.5, 0.6, 0.8 and 1.0 respectively.

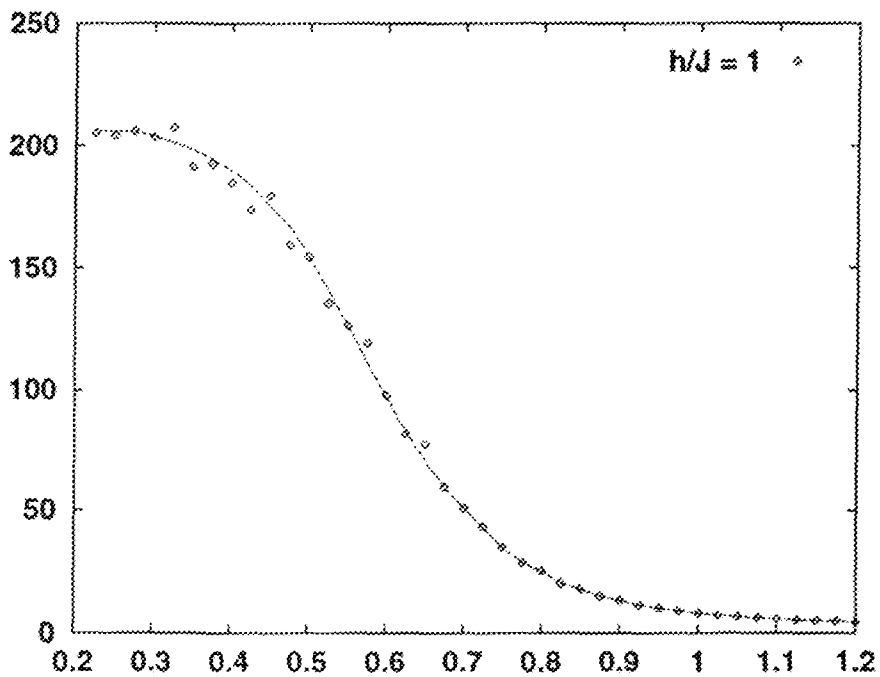

Figure 0.7: Enlarged figure for the case of $h/J = 1$ in Fig. 4.5. The average size of the frozen polar domains in low temperature is similar to that of the chemical domains.

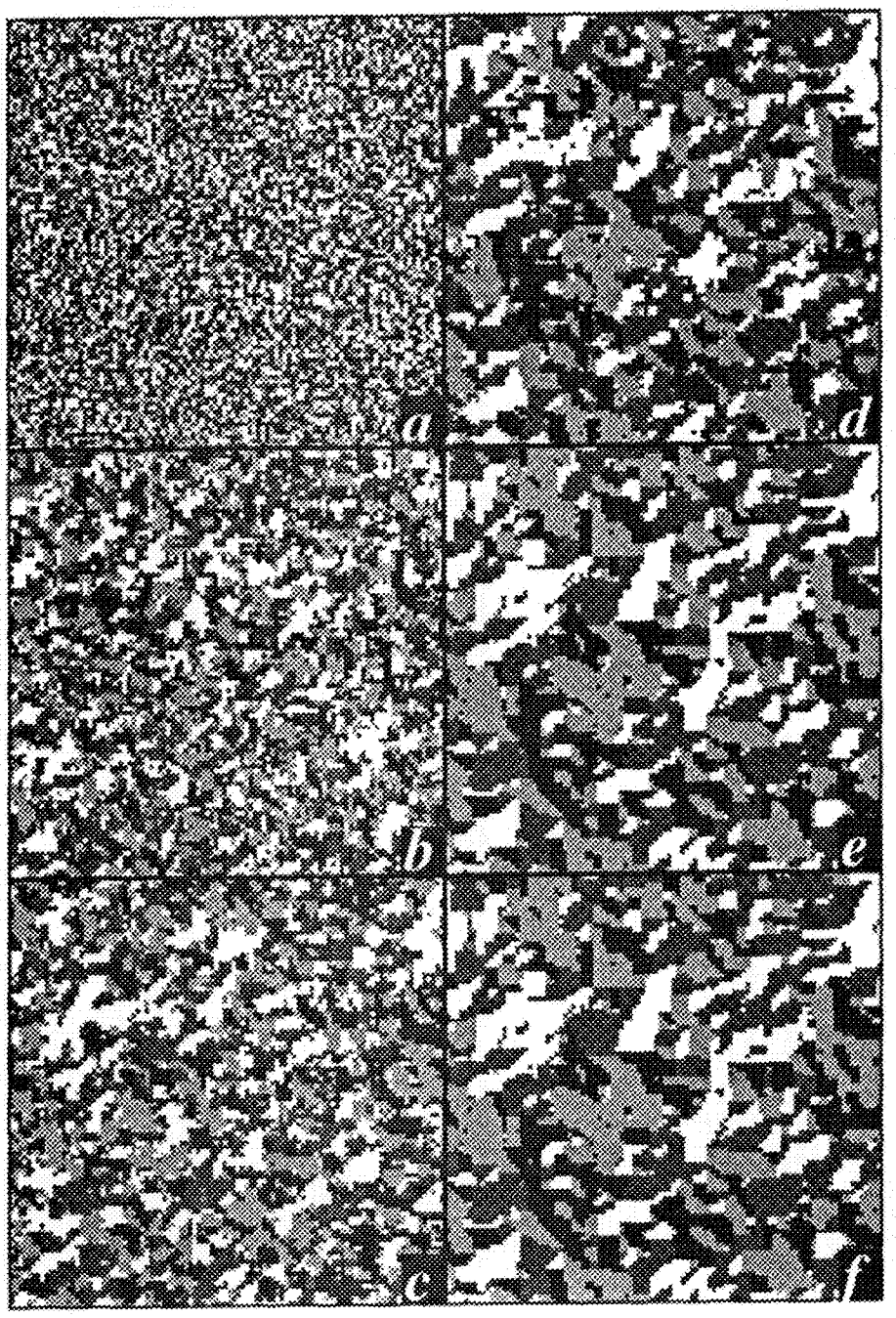

Figure 0.8: The snap-shots of polar moment configurations in the simulation process when $h/J = 1$, which show the evolution of the polar domain textures when the temperature is decreased.

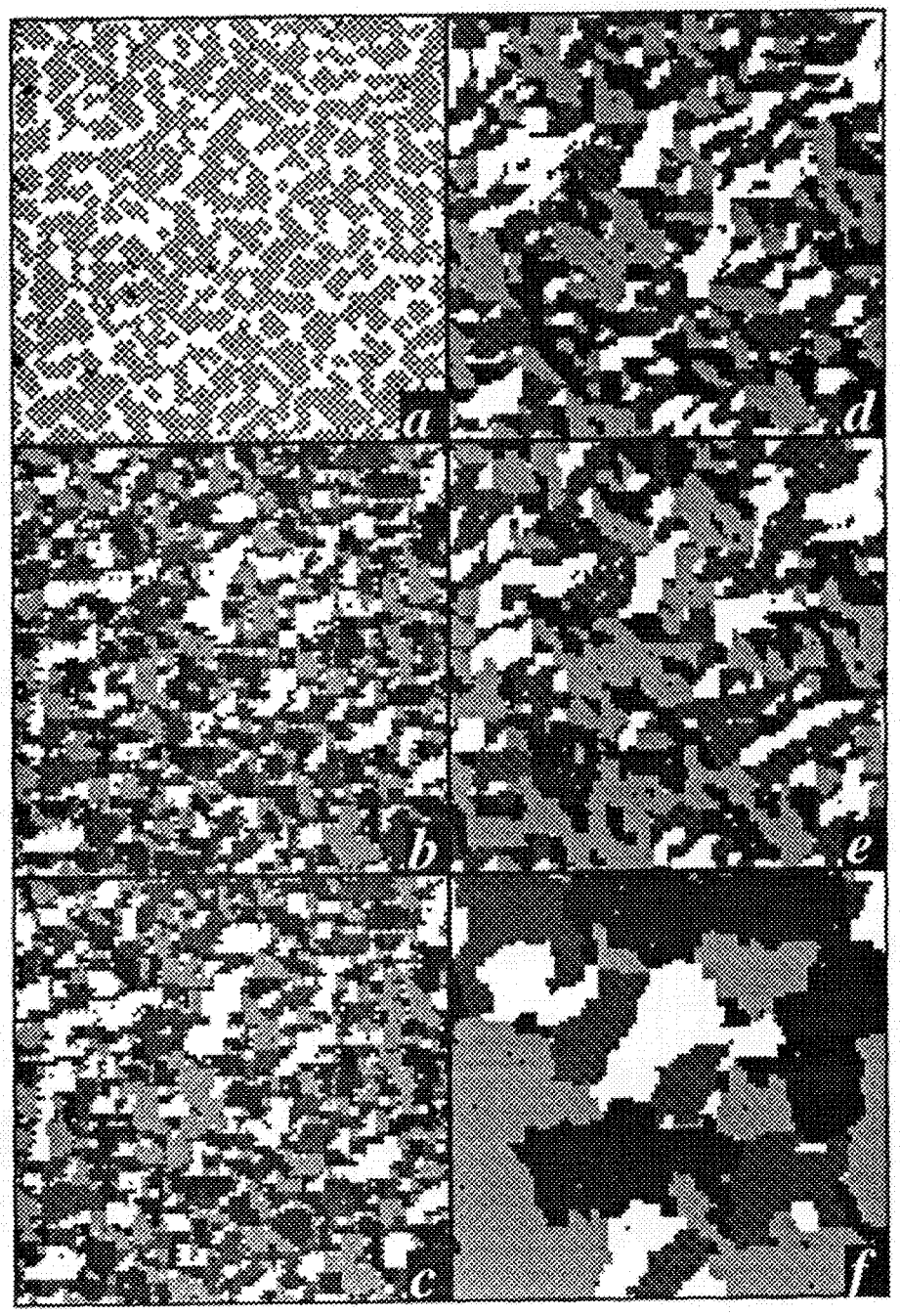

Figure 0.9: Comparison between chemical domain texture and different polar configurations in the frozen polar state at $kT/J = 0.3$ for different values of h/J.